Self-cleaning ceramic tiles coated with Nb_2O_5 doped-TiO_2 nanoparticles

Andre L. da Silva[a,*], Michele Dondi[b], and Dachamir Hotza[a]

[a]*Department of Chemical Engineering (EQA), Graduate Program on Materials Science and Engineering (PGMAT), Federal University of Santa Catarina (UFSC), 88040-900 Florianópolis, SC, Brazil*

[b]*Institute of Science and Technology for Ceramics (ISTEC-CNR), Via Granarolo 64, 48018 Faenza, Italy*

* Corresponding Author. Tel. +55 (48) 99687 2843.

E-mail address: andresilva.urussanga@gmail.com (Andre Luiz da Silva)

Abstract

In this work, 5 mol% Nb_2O_5-doped TiO_2 synthesized sol was sprayed on glazed ceramic tiles. The crystallization of TiO_2 nanoparticles occurs on the surface of the tiles after annealing at 600-900 °C, this innovative approach leads to a drastic decrease in the titania grain size as detected by SEM and XRD. The self-cleaning performance was evaluated using superhydrophilicity that was evaluated by measuring the water contact angle under UV irradiation and by degradation of methylene blue that was carried out according to ISO 10678 and JIS R1703-2. The results showed a high performance of doped samples at all temperatures tested, with a marked dependence on the anatase-to-rutile ratio and crystallite size. At 800 °C, the doped samples achieved water contact angle near to zero in just 15 min of UV irradiation, which confirms the high performance of the self-cleaning ceramic tiles.

Keywords: Ceramic tiles; photocatalytic activity; superhydrophilicity; self-cleaning effect; nanoparticles; titania.

1. Introduction

Photocatalytic (PC) ceramic tiles have been investigated for more than 10 years [1]. Along this period, the ceramic tile industries have been developing new technologies and products. For instance, ink jet printing turned to be widely used, while the tiles tended to be larger with thickness variable over a range never achieved before [2-4]. At the same time, the introduction of functional ceramic tiles with antibacterial, antistatic, water repellent, photoluminescent or self-cleaning properties brought to the final products an added value that goes beyond traditional applications [5].

One of the most desirable properties of a functional ceramic tile is the self-cleaning feature. A ceramic coated with TiO_2 is able to decompose organics under UV light. However, self-cleaning will be efficient if the decontamination rate is higher than the contamination rate [6]. Thus, any increase in performance will have a positive impact on practical applications. Furthermore, the self-cleaning efficiency is increased in external environments, where the material can be exposed to rainfall and water flow. In this case, the superhydrophilic property is also desirable, inducing a low water contact angle, which creates a thin water film, making it possible to wash out the dust that cannot be decomposed. Thus, if these two properties work accordingly, the self-cleaning ceramic tile will present a higher performance [7].

The photoactivity of TiO_2-coated ceramic tiles has been usually evaluated by the degradation of dyes, such as methylene blue (MB) [8-13], orange II [14, 15], rhodamine [1, 8] and crystal violet [8]. Among them, the most common is MB, which is usually tested simultaneously with the measurement of water contact angle [11-13]. These two features are complementary and give valuable information about the self-cleaning performance.

Sintering of TiO_2-coated ceramic tiles is currently carried out by a second firing process at temperatures from 500 to 900 °C. In most cases, when this annealing

temperature is increased, PC performance decreases. Nevertheless, the higher the temperature, the better is the TiO_2 adhesion on the ceramic surface. Furthermore, higher temperatures make the functionalization procedure closer to the industrial tile manufacturing process, which eventually includes a second firing stage for decoration purposes.

The lower performance at higher temperature is usually attributed to the anatase-to-rutile transformation (ART) and to the crystallite coarsening with corresponding drop of specific surface area available for PC reactions [11]. These problems would be possibly minimized using an agent that could simultaneously shift both ART and crystallite growth to higher temperature levels.

Recently, thermodynamic studies with Nb_2O_5-doped TiO_2 have shown that the surface energy decreases as the Nb_2O_5 content increases [16]. Nb_2O_5-doped TiO_2 has also been investigated for photocatalysis. The introduction of Nb_2O_5 in the TiO_2 lattice can stabilize the nanoparticles postponing ART in about 200 °C. Moreover, the crystallite size is decreased and consequently the photocatalytic activity is increased [17]. However, the photocatalytic studies were performed with titania powder dispersed in water, whose performance might be different than that of titania deposited as a thin film [14].

The aim of this work is to evaluate the self-cleaning property of synthesized Nb_2O_5-TiO_2 thin films applied on ceramic tiles. Based on previous investigations, 5 mol% Nb_2O_5 was chosen as the optimal molar percentage of doping. In addition to degradation of methylene blue, superhydrophilicity of coated ceramic tiles was evaluated.

The present work approaches for the first time the production of PC ceramic tiles at temperatures that are commonly used in industrial processes. This technique opens up the possibility to effectively manufacture high effective PC ceramic tiles at industrial scale.

2. Experimental procedures

2.1 Sample preparation

Pure TiO_2 and 5 mol% Nb_2O_5-doped TiO_2 (named as 5NbTi) transparent colloidal suspensions were prepared by the sol gel process. Titanium tetraisopropoxide (TTIP, Sigma-Aldrich, ≥97%) and niobium butoxide (NB, Alfa Aesar, 99%) were used as Ti and Nb precursors, respectively. For doped samples, TTIP and NB were mixed for 10 min forming a homogeneous solution. No partial pre-hydrolyzation was observed in this step. The solution was then slowly dropped into a mixture of ethanol and diethanolamine. The final solution was mixed for 2 h at room temperature. An optimized volume proportion of TTIP (or TTIP/NB), ethanol and diethanolamine (1:5:0.3) was used.

The transparent colloidal solutions were applied on the surface of industrial glazed ceramic tiles by spraying. The samples were left at room temperature for 10 min and then dried for 10 min at 100 °C. Firing was then carried out in a box furnace at 600, 800 and 900 °C with 40 °C/min heating rate for 10 min at the maximum temperature, which simulates a common industrial second firing process.

2.2 Structural characterization

In order to identify the crystalline phases of TiO_2 and 5NbTi powders, a small amount of the colloidal solution was taken, dried at 100 °C for 2 h and calcined at 600, 800 and 900 °C. The oven, heating rate and time at maximum temperature were the same used for sintering the coated ceramic tiles. XRD patterns were acquired using a diffractometer (Bruker D8) in the 20-80° 2θ range, 0.02° scan rate, 16 s per step (LynxEye detector) with Cu*K*α radiation, and λ = 1.5406 Å, operated at 40 kV and 40 mA. A Rietveld refinement was carried out with the aid of a software (Topas

Version 5, Brucker AXS). Crystallite sizes were estimated by the Scherrer equation using a respective software (Diffract.EVA, Brucker AXS).

The surface microstructure and the coating thickness were investigated by SEM (Leica Cambridge Stereoscan 360). The grain size distribution was obtained from particle sizes measurements (using ImageJ 1.50i software) of 200 nanoparticles got from various SEM images. The coating thicknesses were taking from the average of 16 points from the cross section view at different parts of the tiles also using an image treatment software (ImageJ 1.50i).

2.3 Self-cleaning performance

The self-cleaning activity of a ceramic surface is governed by two properties: superhydrophilicity and photocatalytic degradation of organics, which were measured respectively by the water contact angle and the degradation of methylene blue (MB) under UV light. The discussion whether, in these conditions, MB actually undergoes a photocatalytical degradation or just a discoloration by electron delocalization goes beyond the aim of the present work. In any case, even a mere discoloration should be the goal for the application on ceramic tiles.

Superhydrophilicity was determined using a tensiometer (OCA 15, Data Physics Instruments). For each sample, 10 measurements were taken at different points on the surface, and the results were expressed as the arithmetic average. The water contact angle of the sample before irradiation was named zero time and measured in the dark before the experiment. Then, the samples were irradiated under UV-light (Osram Ultra-Vilalux 300 W, light intensity 20 W/m² in the 300-400 nm range) and the measurements were made every 15 min until the angle becomes lower than 5° on average.

The degradation of methylene blue was performed following the ISO 10678:2010 [18]. Firstly, the samples were cleaned with distilled water and dried out at 100 °C

for 30 min. Then, the samples were left under UV radiation (Osram, Ultra-vitalux, 300 W, intensity E = 20 W/m²) for 24 h in order to decompose any possible remaining organic contaminants by photocatalytic oxidation. Then, a 35 mL cylinder was attached on the surface of the samples using silicon glue. The area in contact with the sample was 12.56 cm². In the subsequent step, two identical samples were left in the dark for 24 h with 35 mL of 20 μmol/L aqueous MB solution (conditioning solution) each one. This procedure is necessary because the substrates tend to adsorb the dye molecules. After conditioning, the adsorption solution was replaced by the test solution (35 mL, 10 μmol/L) and the samples were exposed to UV-light (Osram, Ultra-vitalux, 300 W, E = 10 W/m²). The light intensity was measured at the height of the sample underneath the covering glass pane using a UV radiometer (Delta OHM, model HD2302.0 Sonda LP 471 UVA). Thus, the degradation of MB solution was measured every 20 min (up to 3 h) using a spectrophotometer (S-22 UV/Vis, cell length d = 10 mm) by determining the maximum absorption spectrum at 664 nm wavelength. The reference sample (blank) was kept in the dark and the absorption spectrum was also measured at the same time interval.

The specific degradation rate, R, was calculated from Eq. 1.

$$R = \frac{\Delta A_{\lambda} \times V}{\Delta t \times \varepsilon \times d \times A} \qquad (1)$$

where: $\Delta A\lambda$ is the absorption difference from one measurement to another (every 20 min); V is the volume of MB solution; Δt is the time difference; ε is the MB molar extinction coefficient at 664 nm, which is 7402.8 m²/mol; d is the measuring cell length used at the spectrophotometer; and A is the contact area from the MB solution and the catalyst.

The degradation rate R of the irradiated and dark samples makes it possible to calculate the specific photocatalytic activity, P_{MB}, by Eq. 2.

$$P_{MB} = R_{irr} - R_{dark} \qquad (2)$$

Finally, the photonic efficiency, ζ_{MB}, can be calculated using Eq. 3.

$$\zeta_{MB} = \frac{P_{MB}}{E_p} \times 100 \qquad (3)$$

where E_p is the photo UV radiation intensity.

The results are also reported according to the JIS R 1703-2:2007 [19], expressed by the decomposition activity index, *R* (µmol/L/min), represented in this paper as MB Index. The absorbance Abs(t) is converted into concentration of MB after t min, C(t), using a conversion factor K. Since the absorbance is proportional to the concentration (Beer's rule), MB concentration was calculated using the MB molar extinction coefficient of ε (664 nm) = 7402.8 m²/mol in aqueous solution at a concentration of 10.0 ± 0.5 µmol/L [18] as the conversion factor K.
By plotting C(t) as a function of the ultraviolet light irradiation time (min), it is possible to obtain the gradient of the straight line according to the least-squares method. The MB index is then obtained multiplying the gradient by 10^3.

3. Results and discussion

The crystalline phases, powder purity and crystallite sizes were analyzed by X-ray diffraction. The results are shown in Figure 1 and Table 1. XRD patterns of the calcined powders show no sign of contamination. Only anatase and rutile phases are observed in all samples, which attests a high powder purity. At 600 °C, undoped

TiO_2 presents 65 wt% rutile (JCPDS card n. 86-0147) and 35 wt% anatase (JCPDS card n. 71-1167). At the same temperature, 5NbTi is made up of 100 wt% anatase. The average crystallite size of TiO_2 is 25 nm for anatase and 33 nm for rutile, while 5NbTi presents 8 nm of crystallite size on average. At 800 and 900 °C, the anatase-to-rutile phase transition was completed for undoped TiO_2. Rutile was the unique phase observed at those temperatures. The sharp peaks seen in the X-ray patterns make evident the formation of bulk samples with larger crystallite sizes. These values were 56 and 68 nm for 800 and 900 °C, respectively. On the other hand, 5NbTi presented a mix of anatase and rutile phases at 800 °C. Around 38 wt% anatase and 62 wt% rutile, with crystallite sizes of 22 and 25 nm, were respectively obtained. Curiously, the anatase/rutile ratio obtained at 800 °C for 5NbTi and the one obtained at 600 °C for undoped TiO_2 were pretty close. This fact confirms the prediction found in the literature that 5 mol% Nb_2O_5-doped TiO_2 is able to postpone the ART in about 200 °C [17, 20]. At 900 °C, ART was also complete for 5NbTi, while the crystallite size (45 nm) was still smaller than undoped TiO_2 calcined at the same temperature.

It is well reported in the literature that, from the thermodynamic point of view, anatase is more stable than rutile at very small crystallite sizes [21-24]. As the particles grow, at a certain size rutile becomes more stable. This critical crystallite size was determined for undoped TiO_2 as 9 to 67 nm, depending on synthesis method, particle morphology, surface stress and purity. During sintering, the crystallites grow and when the crystal reaches a critical size, the phase transition occurs. Considering that in practice the powders have a size distribution, it is expected that the phase transition happens along a temperature range, which allows all particles to reach the critical size and transform into the most stable phase. The presence of Nb_2O_5 on the surface of TiO_2 can affect the driving forces for particle growth and, at the same time, act as pinning agent, so limiting the growth rate [17].

Thus, if the TiO_2 crystallite growth is hampered, the required temperature to ART will be postponed.

Comparing the surface microstructure under SEM, a significant difference stands out between the TiO_2-coated and 5NbTi-coated ceramic tiles, both annealed at 800 °C (Figure 2). The crystallite sizes distribution of the TiO_2 coating is in the range of 20 to 120 nm, with average of ~65±21 nm (Figure 3a). On the other hand, the 5NbTi coating exhibits a crystallite size distribution in the 12 to 40 nm range, being 24±5 nm on average (Figure 3b). From the catalysis point of view, the advantages are represented by the higher surface area achieved by the doped samples, which provides more active sites for the photocatalytic reaction.

Atanacio *et al.* [25] have shown that niobium has a potential to segregate on the surface of TiO_2. The presence of titanium vacancies, which are formed at the TiO_2/O_2 interface and trapped at the surface, enhances the segregation tendency. Furthermore, the decreasing dimension of crystallites has been attributed to surface segregation [26, 27]. If the dopants segregate on the particle surface, the surface energies will be significantly affected according to Eq. (4).

$$\gamma = \gamma_0 - \Gamma_i(RT \ln X_i^{bulk} + \Delta H_{seg}) \quad (4)$$

where: γ_0 is the surface energy of the undoped compound; Γ_i is the surface excess of component *I*; *R* is the constant gas; *T* is the temperature; X_i^{bulk} is the *i* content in the bulk material; and ΔH_{seg} is the enthalpy of segregation of compound *i*.

A nanostructure stability map based on the effect of the enthalpy of segregation on the grain boundary energy has been defined using Eq. (4). Grain boundary energy is the main driving force for grain growth in addition to the curvature of the interface.

Therefore, by adding dopants prone to segregate at the boundaries, a stable nanostructure could be achieved inhibiting the crystallite growth [28].

Figures 2c and 2d show the cross-section view of the TiO_2-coated ceramic tiles and 5NbTi-coated ceramic tiles, respectively. It is seen that, even though the tile surface is not completely flat, the titania layer covers completely the ceramic surface, forming a homogeneous coating. The TiO_2 coating presented a thickness of 265±56 nm, while the 5NbTi coating was 223±49 nm thick. Even though the TiO_2 coating has presented a thickness slightly higher than the 5NbTi, both values are considered equivalent, because the difference between them is inside the dispersion error. In any case, the titania thickness obtained in this work can be considered very low and it is attributed to the deposition method. According to literature data, the spray technique provides thickness from 0.1 to 3.0 μm [8, 10, 29], while other methods go much higher. For instance, ink jet and roller printing reach thicknesses of ~70 μm and ~100 μm, respectively [13]. The advantages of having a thin layer are not only related to a very small amount of powders. A transparent thin film formed by TiO_2 nanoparticles can give remarkable photocatalytic properties and at the same time it preserves the aesthetic characteristics of the ceramic tiles.

Figure 4 shows the water contact angle of TiO_2 and 5NbTi-coated ceramic tiles annealed at 600 °C (Fig. 4a), 800 °C (Fig. 4b) and 900 °C (Fig. 4c). At 600 °C, both samples presented water contact angle <5° after just 20 min of UV irradiation. No difference in terms of performance is observed between the samples at this temperature. After annealing at 800 °C, the TiO_2 coating took ~40 min under UV to exhibit superhydrophilicity. However, for the same annealing temperature, the water contact angle of 5NbTi went <5° in just 15 min, which is the best result achieved in this work. The TiO_2 coating annealed at 900 °C did not show any decrease in water contact angle along 2 h of testing, since data remained within the standard deviation.

On the other hand, 5NbTi-coated ceramic tiles are still active after annealing at 900 °C, reaching water contact angle <5 ° in 2 h.

The specific photocatalytic activity, P_{MB}, is shown in Figure 5. Table 2 presents the absolute values for P_{MB}, photonic efficiency (ζ_{MB}) and MB index. The P_{MB} and ζ_{MB} are the standard expression of photoactivity according to ISO 10678 [18] and the MB index is the standard photocatalytic representation according to JIS R 1703-2 [19]. The trend is similar regardless the method used. It is clearly observed that the 5NbTi coating exhibits a photocatalytic activity higher than TiO_2 at all temperatures tested. In particular, the best performance was achieved at 600 °C. Overall, the photoactivity decreases as the temperature increases for both samples, making evident the effect of the crystallite growth and phase transition. In fact, both the TiO_2 coated sample annealed at 600 °C and the 5NbTi one annealed at 800 °C have a similar performance and, coincidently, almost the same anatase/rutile ratio. This example makes evident the benefit of the ART shift to higher temperature. For the ceramic tile manufacturing, this is very important, since the titania doping allows firing at higher temperatures without any performance loss. The simultaneous presence of rutile and anatase can be even beneficial since it promotes the electron transport to the conduction band of rutile phase, when adjacent to anatase phase, decreasing the recombination rate. Thus, the presence of rutile may act as a defect or impurity, fostering a higher photocatalytic activity [30]. After annealing at 900 °C, the photoactivity of the TiO_2 coating was very low, to the point it cannot be considered photoactive anymore. On the other hand, 5NbTi was still active, proving one more time the advantage ensured by the Nb_2O_5 doping on TiO_2 nanoparticles.

One of the facts responsible for the higher performance of 5NbTi coating with respect to undoped TiO_2 coating is the smaller crystallite size of the photoactive sites achieved by doping, which provide a higher surface area. However, in our previous work [17], we have shown that even considering the same surface area, the samples

doped with Nb_2O_5 are distinguished by a photocatalytic activity higher than undoped TiO_2.

The ionic radius (in octahedral coordination) of Nb^{5+} is 0.64 Å, which is slightly larger than that of Ti^{4+} (0.605 Å). Hence, the $(Ti,Nb)O_2$ solid solution implies an excess charge due to Nb^{5+} in substitution to Ti^{4+}, which can be compensated by the mechanisms illustrated through Eq. (4) and Eq. (5). The first possibility is the creation of Ti^{4+} cation vacancy for every 4 Nb^{5+} cations. Another option is the reduction of Ti^{4+} to Ti^{3+} for every Nb^{5+} incorporated, where O^{2-} is oxidized [31-33]. The reduction is less energetic than vacancy formation. Thus, from the thermodynamic point of view, Eq. (4) is more favorable. The presence of active Ti^{3+} sites on the surface could act as sites for trapping photogenerated electrons that could effectively inhibit the recombination of photoinduced electrons and holes [34].

$$\frac{1}{2}Nb_2O_5 \xrightarrow{TiO_2} Nb_{Ti}^{\cdot} + \frac{1}{4}V_{Ti}^{''''} + \frac{5}{2}O_O^X \quad (4)$$

$$\frac{1}{2}Nb_2O_5 \xrightarrow{TiO_2} Nb_{Ti}^{\cdot} + Ti^{(3+)'}_{Ti^{(4+)}} + 2O_O^X + \frac{1}{4}O_2 \quad (5)$$

In addition, Nb-doped TiO_2 can present better charge separation. Nb-doping introduces shallow donor levels below the CB edge, which can act as electron traps to retard electron-hole recombination. Thus, the lifetime of photogenerated electrons and holes can be increased and consequently the photocatalytic efficiency is enhanced [31]. Moreover, Nb_2O_5 itself shows high photocatalytic decomposition of methylene blue [35]. Considering that Nb_2O_5 has a potential to segregate on the surface of TiO_2 [25], the major part of Nb_2O_5 doping is on the surface of TiO_2,

which could explain the photoactivity achieved at 900 ° for 5NbTi even if at that temperature the anatase-to-rutile phase transition is completed.

Table 1. Anatase and rutile relative amounts and crystallite sizes.

Sample	**Annealing Temperature (°C)**	**Anatase (wt%)**	**Anatase crystallite size (nm)**	**Rutile (wt%)**	**Rutile crystallite size (nm)**
TiO_2	600	35	25	65	33
5NbTi	600	100	8	0	--
TiO_2	800	0	--	100	56
5NbTi	800	38	22	62	25
TiO_2	900	0	--	100	68
5NbTi	900	0	--	100	45

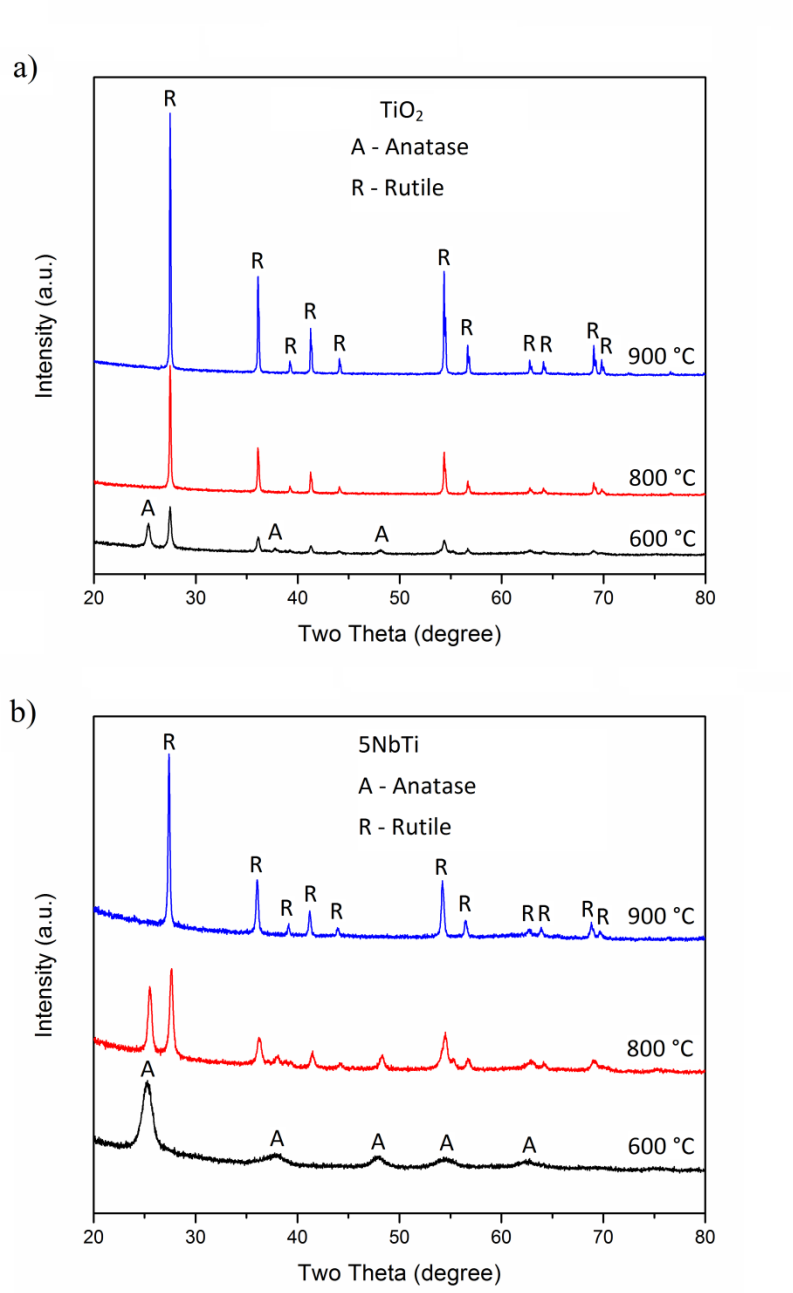

Figure 1. X-ray diffraction patterns of (a) TiO_2 and (b) 5NbTi, after heat treatment at 600, 800 and 900 °C.

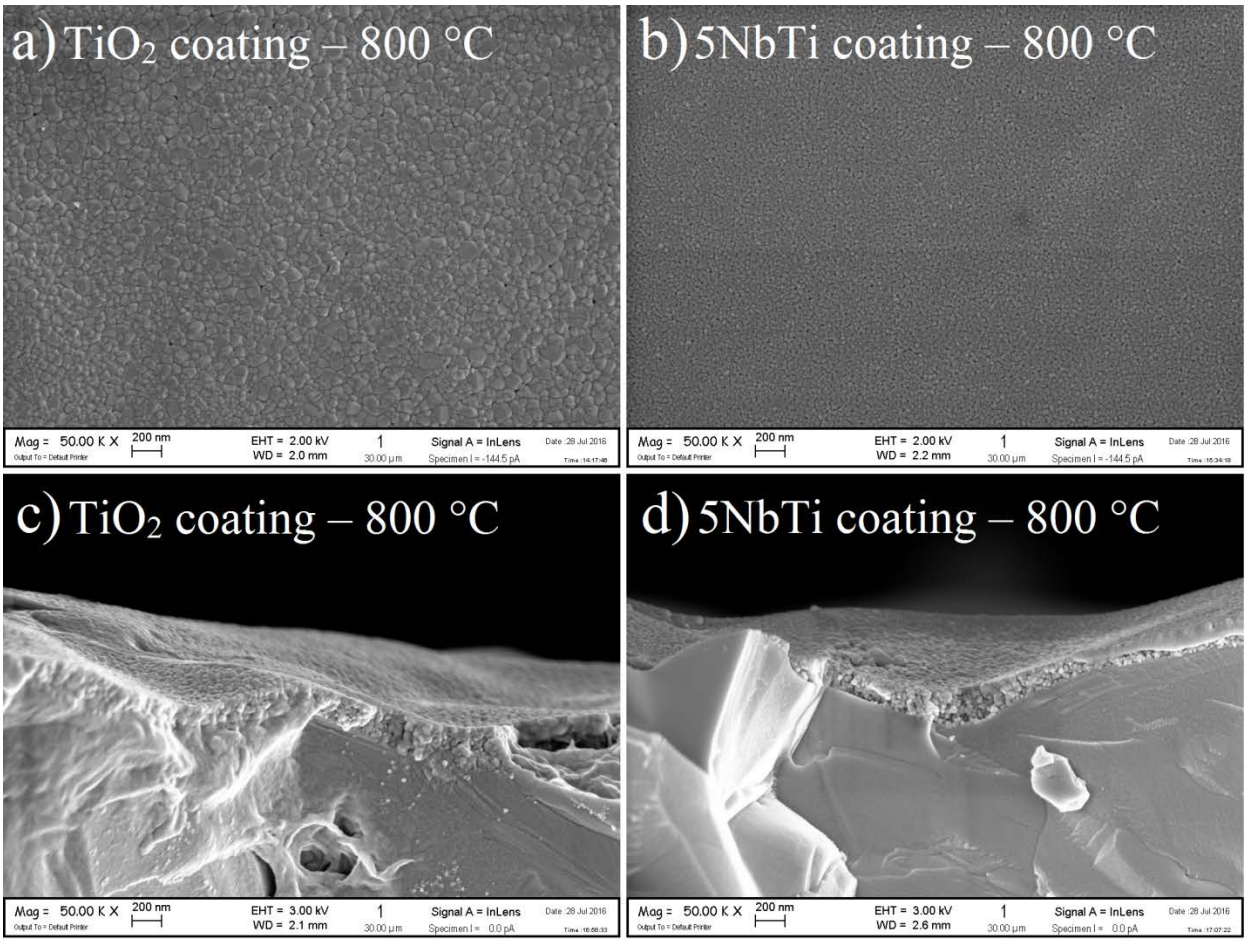

Figure 2. SEM images of coated ceramic tiles annealed at 800 °C: (a) TiO_2 coated ceramic tiles surface. (b) 5NbTi coated ceramic tiles surface. (c) Cross-section view of TiO_2 coating. (d) Transversal view of 5NbTi coating.

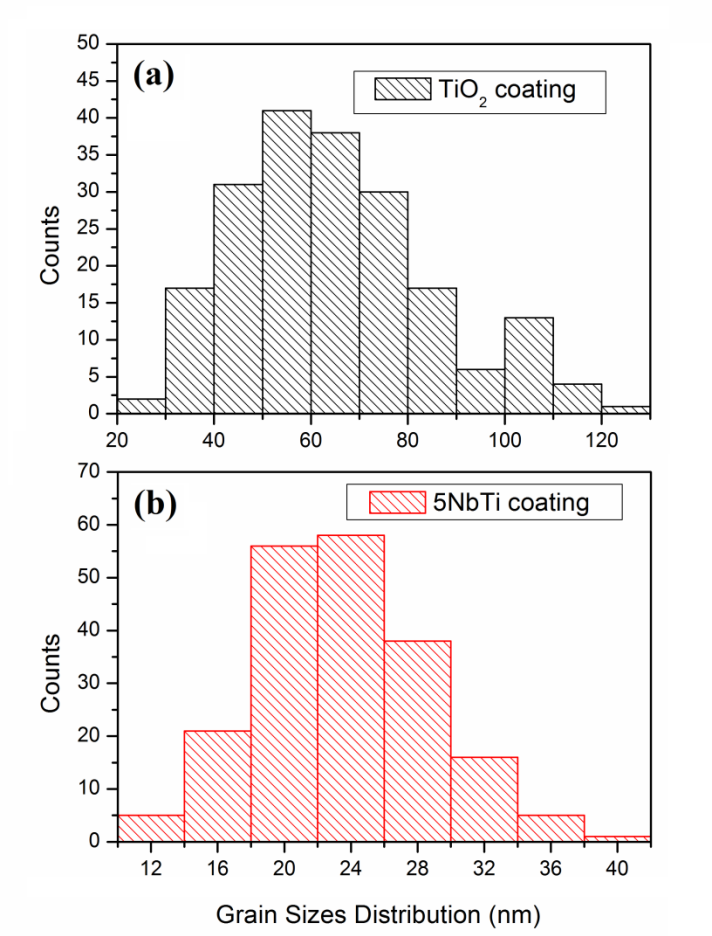

Figure 3. Grain size distribution of TiO_2 coated on ceramic tiles annealed at 800 °C: (a) TiO_2coating. (b) 5NbTi coating.

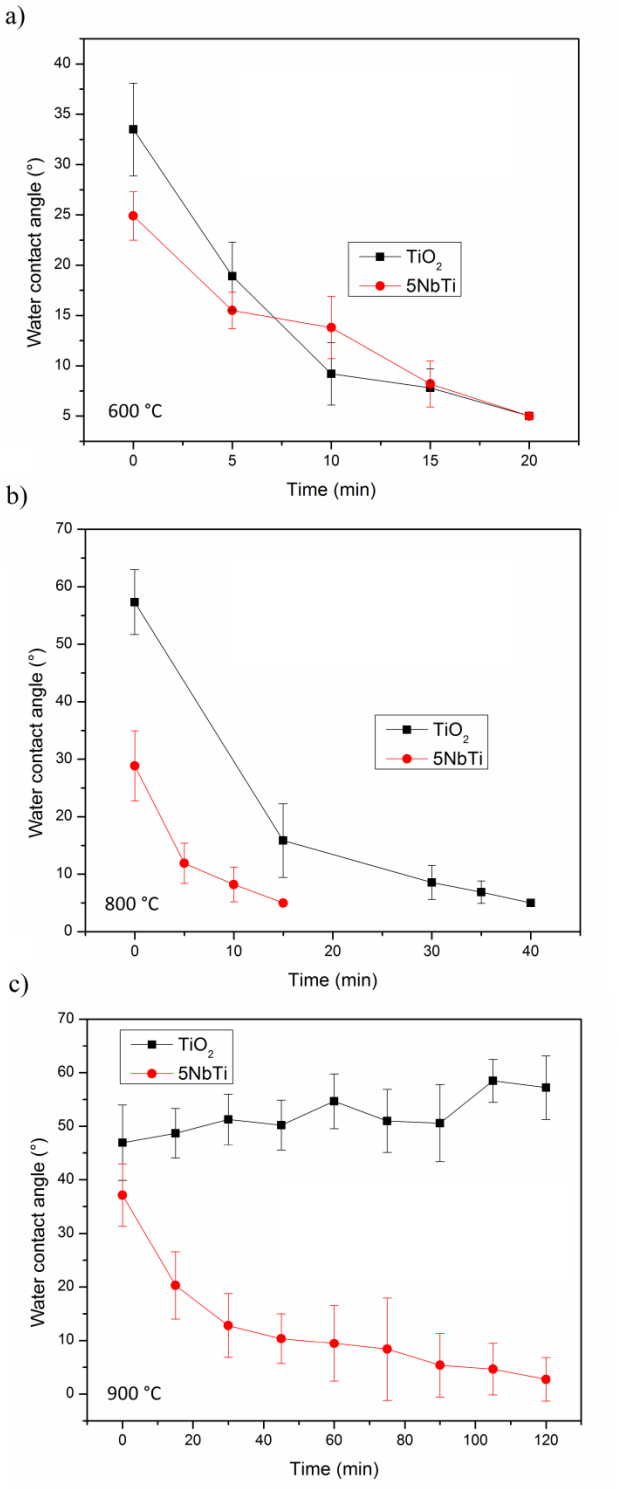

Figure 4. Water contact angle under UV-light irradiation for TiO_2-coated ceramic tiles and 5NbTi-coated ceramic tiles at different temperatures: (a) 600 °C. (b) 800 °C. (c) 900 °C.

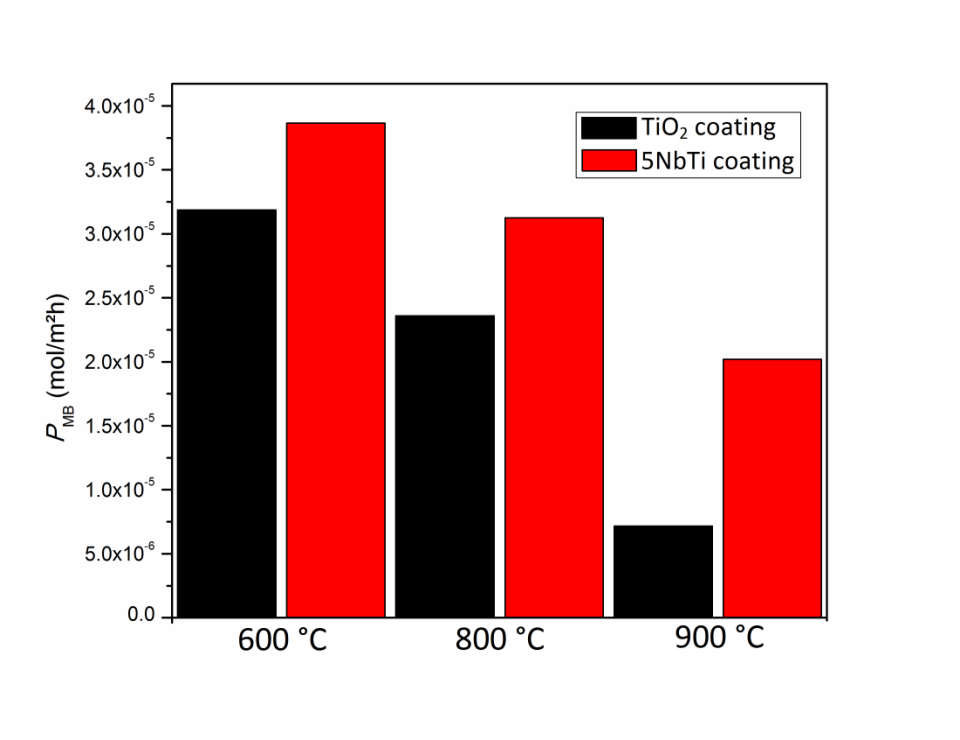

Figure 5. Specific photocatalytic activity (P_{MB}) for TiO_2-coated ceramic tiles and 5NbTi-coated ceramic tiles annealed at 600, 800 and 900 °C.

Table 2. Specific photocatalytic activity (P_{MB}), photonic efficiency (ς_{MB}) and MB Index (JIS R 1703-2:2007).

Sample	**Temperature (°C)**	**P_{MB} (mol/m²*h)**	**ς_{MB} (%)**	**MB Index**
TiO_2 coating	600	3.19E-05	0.0296	18.6
5NbTi coating	600	3.86E-05	0.0359	23.3
TiO_2 coating	800	2.36E-05	0.0223	14.7
5NbTi coating	800	3.12E-05	0.0293	18.7
TiO_2 coating	900	7.15E-06	0.0067	3.8
5NbTi coating	900	2.02E-05	0.0188	11.9

4. Conclusions

Self-cleaning ceramic tiles were successfully produced by spray coating of 5 mol% Nb_2O_5-doped TiO_2 synthesized sol gel suspensions. Thin films were obtained (~250 nm) making it possible to produce self-cleaning ceramic tiles using a very low amount of nanopowder. X-ray diffraction of the powders showed only anatase and rutile crystalline phases. No sign of second phases was detected. SEM images allowed to detect the crystallite size stabilization of the doped samples. At 800 °C, TiO_2 presented crystallite size of ~64.8 nm on average, while for 5NbTi it was ~23.6 nm. The photocatalytic performance of doped samples was higher at all temperature tested. Even at 900 °C, the coated samples were photoactive, while the undoped samples were not photoactive anymore.

Acknowledgments

The authors gratefully acknowledge the Brazilian funding agency CNPq (Process numbers 401451/2012-7 and 207445/2015-0).

REFERENCES

1. T. Kemmitt, N.I. Al-Salim, M. Waterland, V.J. Kennedy, A. Markwitz, Photocatalytic titania coating, Curr. Appl. Phys. 4 (2004) 189-192.
2. A.L. da Silva, J. Feltrin, M. Dal Bó, A.M. Bernardin, D. Hotza, Effect of reduction of thickness on microstructure and properties of porcelain stoneware tiles, Ceram. Int. 40 (2014) 14693-14699.
3. A.L. da Silva, A.M. Bernardin, D. Hotza, Forming of thin porcelain tiles: A comparison between tape casting and dry pressing, Ceram. Int. 40 (2014) 3761-3767.
4. M. Montorsi, C. Mugoni, A. Passalacqua, A. Annovi, F. Marani, L. Fossa, R. Capitani, T. Manfredini, Improvement of color quality and reduction of defects in the ink jet-printing technology for ceramic tiles production: A Design of Experiments study, Ceram. Int. 42 (2016) 1459-1469.
5. S.D. Majumdar, S. Kumar, V.T. Mathew, S. Saha, Functional Ceramic Tiles, Trans. Ind. Ceram. Soc. 69 (2010) 37-44.
6. A. Fujishima, X. Zhang, D.A. Tryk, TiO_2 photocatalysis and related surface phenomena, Surf. Sci. Rep. 63 (2008) 515-582.

7. R. Wang, K. Hashimoto, A. Fujishima, M. Chikuni, E. Kojima, A. Kitamura, M. Shimohigoshi, T. Watanabe, Photogeneration of Highly Amphiphilic TiO_2 Surfaces, Adv. Mater. 10 (1998) 135-138.
8. V. Petrovič, V. Ducman, S.D. Škapin, Determination of the photocatalytic efficiency of TiO_2 coatings on ceramic tiles by monitoring the photodegradation of organic dyes, Ceram. Int. 38 (2012) 1611-1616.
9. V. Ducman, V. Petrovič, S.D. Škapin, Photo-catalytic efficiency of laboratory made and commercially available ceramic building products, Ceram. Int. 39 (2013) 2981-2987.
10. S. Ke, X. Cheng, Q. Wang, Y. Wang, Z. Pan, Preparation of a photocatalytic $TiO_2/ZnTiO_3$ coating on glazed ceramic tiles, Ceram. Int. 40 (2014) 8891-8895.
11. V.B. Tezza, M. Scarpato, L.F.S. Oliveira, A.M. Bernardin, Effect of firing temperature on the photocatalytic activity of anatase ceramic glazes, Powder Technol. 276 (2015) 60-65.
12. C. Sciancalepore, F. Bondioli, Durability of SiO_2–TiO_2 photocatalytic coatings on ceramic tiles, Int. J. Appl. Ceram. Tec. 12 (2015) 679-684.
13. M. Raimondo, G. Guarini, C. Zanelli, F. Marani, L. Fossa, M. Dondi, Printing nano TiO_2 on large-sized building materials: Technologies, surface modifications and functional behaviour, Ceram. Int. 38 (2012) 4685-4693.
14. M.P. Seabra, R.R. Pires, J.A. Labrincha, Ceramic tiles for photodegradation of Orange II solutions. Chem. Eng. J. 171 (2011) 692-702.
15. E. Rego, J. Marto, P. São Marcos, J.A. Labrincha, Decolouration of Orange II solutions by TiO_2 and ZnO active layers screen-printed on ceramic tiles under sunlight irradiation, Appl. Cat. A-Gen. 355 (2009) 109-114.
16. A.L. da Silva, D. Hotza, R.H.R. Castro, Surface energy effects on the stability of anatase and rutile nanocrystals: A predictive diagram for Nb_2O_5-doped-TiO_2, Appl. Surf. Sci. 393 (2017) 103-109.
17. A.L. da Silva, D. Muche, S. Dey, D. Hotza, R. Castro, Photocatalytic Nb_2O_5-doped TiO_2 nanoparticles for glazed ceramic tiles, Ceram. Int. 42 (2016) 5113-5122.
18. ISO, *International Standard ISO 10678-Fine Ceramics (Advanced Technical Ceramics) - Determination of Photocatalytic Activity of Surfaces in an Aqueous Medium by Degradation of Methylene Blue.* . 2010.
19. *JIS R 1703-2 Fine ceramics (advanced ceramics, advanced technical ceramics) - Test method for self-cleaning performance of photocatalytic materials - Part 2: Decomposition of wet methylene blue*. 2007.
20. E. Traversa, M.L.D. Vona, S. Licoccia, Sol-Gel processed TiO_2-based nano-sized powders for use in thick-film gas sensors for atmospheric pollutant monitoring, J. Sol-Gel Sci. Techn. 22 (2001) 167-179.
21. H. Zhang, J.F. Banfield, Thermodynamic analysis of phase stability of nanocrystalline titania. J. Mater. Chem. 8 (1998) 2073-2076.
22. A.S. Barnard, P. Zapol, Effects of particle morphology and surface hydrogenation on the phase stability of TiO_2, Phys. Rev. B, 70 (2004) 235403.
23. A.A. Levchenko, G. Li, J. Boerio-Goates, B.F. Woodfield, A. Navrotsky, TiO_2 stability landscape: polymorphism, surface energy, and bound water energetics, Chem. Mater. 18 (2006) 6324-6332.
24. R.H.R. Castro, B. Wang, The hidden effect of interface energies in the polymorphic stability of nanocrystalline titanium dioxide, J. Am. Ceram. Soc. 94 (2011) 918-924.
25. A.J. Atanacio, T. Bak, J. Nowotny, Niobium segregation in niobium-doped titanium dioxide (rutile), J. Phys. Chem. C, 118 (2014) 11174-11185.
26. R.H.R. Castro, J. Rufner, P. Hidalgo, D. Gouvêa, J.A.H. Coaquira, K. van Benthem, Surface segregation in chromium-doped nanocrystalline tin dioxide pigments, J. Am. Ceram. Soc. 95 (2012) 170-176.

27. C-H. Chang, M. Gong, S. Dey, F. Liu, R.H.R. Castro, Thermodynamic stability of SnO_2 nanoparticles: the role of interface energies and dopants, J. Phys. Chem. C, 119 (2015) 6389-6397.
28. R.H.R. Castro, On the thermodynamic stability of nanocrystalline ceramics, Mater. Lett. 96 (2013) 45-56.
29. F. Bondioli, R. Taurino, A.M. Ferrari, Functionalization of ceramic tile surface by sol–gel technique, J. Colloid Interf. Sci. 334 (2009) 195-201.
30. A.M. Ferrari-Lima, R.G. Marques, M.L. Gimenes, N.R.C. Fernandes-Machado, Synthesis, characterisation and photocatalytic activity of N-doped TiO_2–Nb_2O_5 mixed oxides, Catal. Today, 254 (2015) 119-128.
31. J. Yang, X. Zhang, C. Wang, P. Sun, L. Wang, B. Xia, Y. Liu, Solar photocatalytic activities of porous Nb-doped TiO_2 microspheres prepared by ultrasonic spray pyrolysis, Sol. St. Sci. 14 (2012) 139-144.
32. N.R. Elezović, B.M. Babic, Lj. Gajic-krstajic, V. Radmilovic, N.V. Krstajic, L.J. Vracar, Synthesis, characterization and electrocatalytical behavior of Nb–TiO_2/Pt nanocatalyst for oxygen reduction reaction, J. Power Sources, 195 (2010) 3961-3968.
33. J. Arbiol, J. Cerda, G. Dezanneau, A. Cirera, F. Peiro, Effects of Nb doping on the TiO_2 anatase-to-rutile phase transition, J. Appl. Phys. 92 (2002) 853-861.
34. Z. Wan, G-F. Huang, W-Q Huang, C. Jiao, X-G. Yan, Z-M Yang, Q. Zhang, The enhanced photocatalytic activity of Ti^{3+} self-doped TiO_2 by a reduction method, Mater. Lett. 122 (2014) 33-36.
35. Y. Zhao, X. Zhou, L. Ye, S.C.E. Tsang, Nanostructured Nb_2O_5 catalysts, Nano Reviews, 3 (2012) 17631.